UITS Journal of Sciences & Engineering ❖ Volume-10, Issue-1
ISSN: 2521-8107; March 2024

Effect of Iron Doping on Structural, Optical and Electrical Properties of Nanostructured Tungsten Oxide Thin Films for Biosensor Applications

* Muslima Zahan[1], Jiban Podder[2]

ABSTRACT : ***Nanostructured Tungsten Oxide (WO_3) and Iron (Fe) doped Tungsten Oxide (Fe:WO_3) thin films were synthesized by a simple spray pyrolysis technique at 450 ^{0}C substrate temperature onto the plain glass substrate. The surface morphological, structural, optical, electronic and glucose sensing effects of the deposited thin films were explored varying with 2, 4, 6, 8, and 10 at% Fe concentrations . Scanning Electron Microscope images revealed a an uniform, densed and porous surface morphology of WO_3 and Fe:WO_3 thin films. Structure of the prepared films were analyzed by X-Ray Diffraction patterns and observed monoclinic crystal structure having lattice constants a = 7.273 Å, b = 7.548 Å and c = 7.697 Å are well matched with (JCPDS card No.043-1035. The band gap energy for undoped WO_3 nanoparticles has been observed to be 2.72 eV which is increased to 2.99 eV and 3.03 eV at 2 at % and 4 at% Fe doping and is decreased to 2.88eV, 2.79 eV and 2.74 eV with , 6 at%, 8 at% Fe and 10 at% Fe doping, respectively. The glucose sensing properties revealed that Fe doping greatly improve the sensing properties of WO_3 thin film and the highest glucose-sensitivity was found about 43% and fast response time was about 0.97 sec for 6 at % Fe:WO_3 thin film.***

Keywords: Thin film; Nanostructure; Fe doped WO_3; SEM; XRD; Biosensor.

1. INTRODUCTION

In the recent years, the benefits of transition metal oxides have been exploited in many challenging fields of information science, nano and micro-electronics, computer science, energy, transportation, safety engineering, military technologies, optoelectronic, electrochromic devices, etc. [1-2].

1 Lecturer, Department of EEE, UITS
* Corresponding Author: Email: muslima.zahan@uits.edu.bd
2 Professor, Department of Physics, BUET
Email: jpodder59@gmail.com

Among them one of the most interesting and novel properties of tungsten oxide (WO_3) is applied in advanced technological applications, because of a unique physical and chemical properties, structural transformation and sub stoichiometric phase transitions and a wide band gap oxide semiconductor properties. It attracted the more attention of researchers to explore their applications in the fields of in electrochromic devices, semiconductor gas sensors and pholtocatalysis and biosensor devices [3-4]. Nanostructured tungsten trioxide, WO_3 is temperature dependent. It is tetragonal at temperatures above 740 °C, orthorhombic from 330 to 740 °C, monoclinic from 17 to 330 °C, and triclinic from 50 to 17 °C. The most common structure of WO_3 is monoclinic. The monoclinic WO_3, on the other hand, is completely oxidized, and therefore has a better catalytic activity [5-6] Tungsten trioxide is used for many purposes in everyday life. It is frequently used in industry to manufacture tungstate for x-ray screen phosphors, for fireproofing fabrics and in gas sensors.

Due to its rich yellow color, WO_3 is also used as a pigment in ceramics and paints. WO_3 has attracted a great deal of interest in the last few years for bio sensing applications. WO_3 is a n-type semiconducting material with a wide band ga-. Its band-gap energy has been mainly measured by optical absorption, varying from about 2.6 to 3.0 eV.[7-8] The band gap of WO_3 is certainly of interest for both applied and fundamental aspects. Till today substantial developments are attained in the controlled synthesis of WO_3 thin films. Many efforts have given to synthesize WO_3 and Fe:WO_3 thin film as chemical bath deposition, sputtering, spray pyrolysis, pulsed laser deposition, chemical vapor deposition, sol-gel, dip coating and hydrothermal method [9-11]. Among these various deposition techniques, the spray pyrolysis deposition technique is more suitable because of simplicity, easy to control, low cost, and scope of large area deposition. Very few reports are available in the literature on optical, structural, and electrical properties of Fe:WO_3 thin films for Biosensing performance. The aim of this work is to find out the surface morphological, structural, optical and electronic properties of WO_3 thin films synthesized via spray pyrolysis method and to see the effect of Fe doping concentrations suitability for glucose sensor.

2. MATERIALS AND METHODS

Fe:WO_3 thin films were synthesized by a spray pyrolysis technique. The analytical grade Tungstic acid (H_2WO_4) powder ((Merck, Germany, 98% extra pure), Ammonium ceric nitrate [$(NH_4)2Ce\ (NO_3)_6$] salt (Merck, Germany, 99% purity), Ferric chloride ($FeCl_3$) were used as mother precursor for W and Fe sources respectively.

Deionized distilled water was used as a solvent. Ethanol (C_2H_5OH) and hydrochloric acid (HCl) were used as a reagent to control the pH value. The plain glass slide of area 5 × 2.5 cm^2 with a suitable mask was used as a substrate. The compressed dry air was used as a carrier gas. D-glucose ($C_6H_{12}O_6$) and sodium hydroxide (NaOH) were used as precursors for sensitivity measurements.

The substrates were cleaned with acetone and distilled water in an ultrasonic cleaner for 30 min and subsequently dried in flowing hot air to execute a better adherence in the middle of the film and the substrate. After that, the solution was filtered and then sprayed through a fine bore in the form of fine droplets on pre-heated commercial glass substrates with a deposition time of 20 min. The deposition process was carried out at 450 °C constant substrate temperature. The substrate was put at a 25 cm distance from the spray nozzle. The air pressure was controlled by 0.5 bar as the carrier. 0.5 mL solution was maintained per minute as the spray rate throughout the experiment. The deposited thin films were allowed to cool to room temperature. The as-deposited WO_3 thin films were found homogeneous.

3. RESULTS AND DISCUSSION

3.1. Surface morphological analysis

The Scanning Electron Microscopic images of WO_3 and 2, 4, 6, 8 and 10 at% Fe doped WO_3 thin films observed at X 10000, 5.0 kV show that the substrates are uniformly covered with spherical nanoparticles indicated in Figure-1. The regular distribution of grains is attributed all over the surface. The particle size increase with Fe concentration up to 8 at % and the agglomeration of the particles decreased which may be attributed to both the oxidation of surface-adsorbed water molecules and the structural transformation of WO_3 that accompanies the loss of water molecules as vapor [12]. The particles decrease at 10 at% Fe concentration. The surface remains homogeneous and smooth up to 4 at % iron. At 8 and 10 at % Fe doping some crakes are observed over the surface which may due to oxidation of Fe^{+3} ions on the surface. The reason for the formation of crakes may be due to the evaporation of solvent (H_2O) from the film [10]. It is seen from the SEM images that 4 at% Fe doped WO_3 surface is more porous which may be suitable for biosensing applications. In Figure 1 SEM images with EDX spectra of 0 at%, 4at% and 8 at% Fe doped WO_3 thin films are displayed.

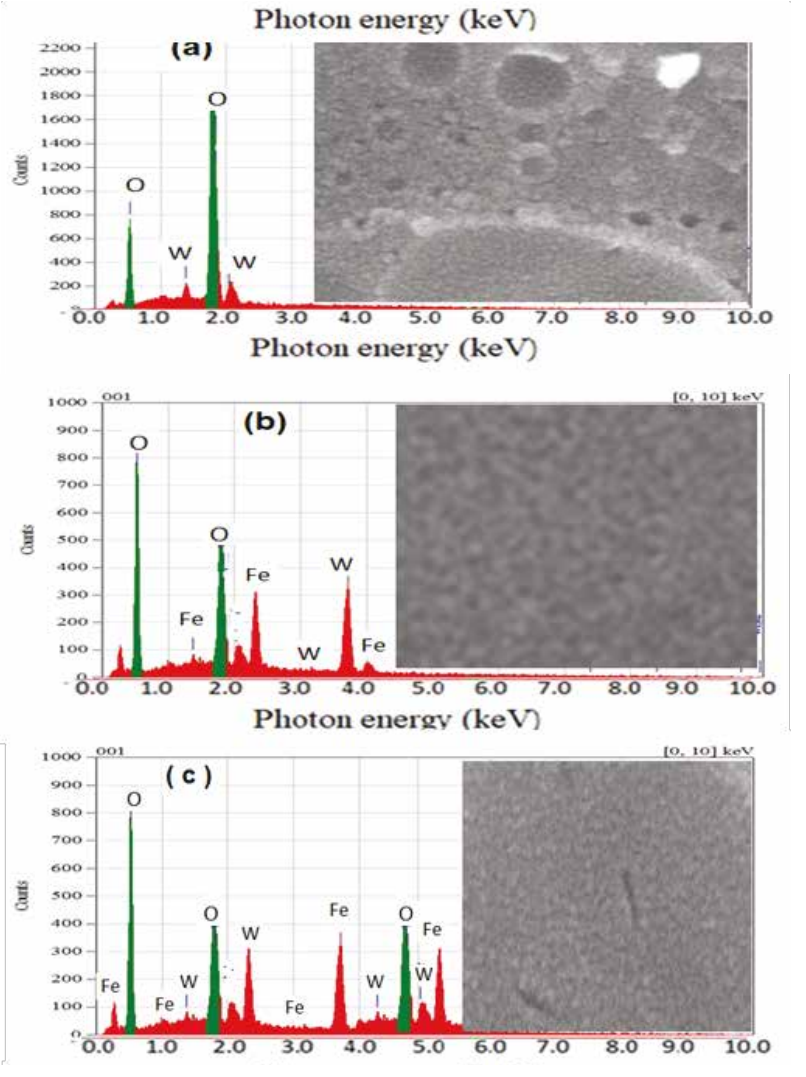

Figure 01: SEM images with EDX spectra of 0 at%, 4at% and 8 at% Fe:WO_3 thin films.

3.2. Compositional analysis

EDX analysis confirmed the elements of the compositions of pure WO_3 and Fe doped WO_3 thin films. EDX data have been collected at various points on the scan area. EDX data support the uniformity of the synthetic distribution of the prepared thin films. Different peaks corresponding to W and O were found in the spectrum, which confirms the WO_3 thin film and peak for the composition of W, Fe and O indicate the Fe doped WO_3 thin films shown in Figure 2.

Amount of W reduces with the increment of Fe concentration in Fe doped WO_3 thin films. The EDX data supported the logical substitution of W caused by Fe doping. The EDX reports are displayed in Figure 2.

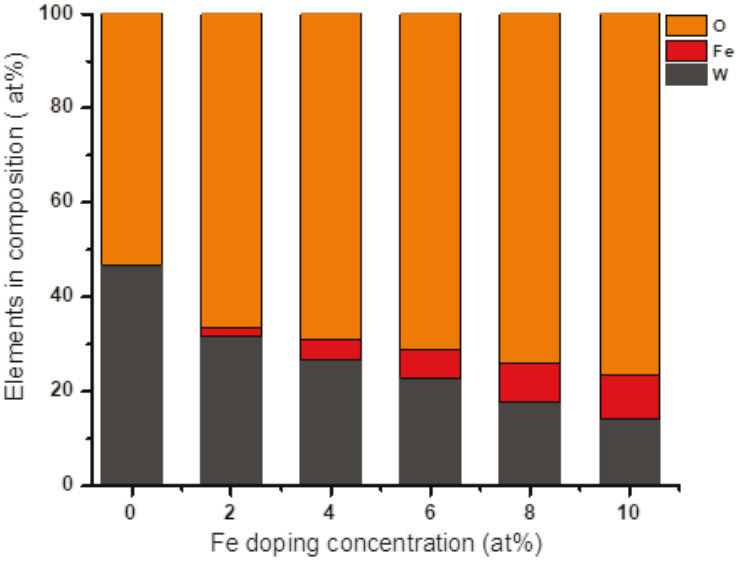

Figure 02: Quantitative analysis from EDX spectra of 0-10 at% Fe doped WO_3 thin film.

3.3. Structural properties

The crystallographic structure of the prepared samples were characterized by XRD. Figure 3 shows the XRD patterns of Fe:WO_3 films at different Fe concentrations of 0, 2, 6,8 and 10 at%, respectively. The observed diffraction peaks are well matched with the monoclinic WO_3 crystal structure (JCPDS card No.043-1035 [13-14] having lattice constants a = 7.273 Å, b = 7.548 Å and c = 7.697 Å. With Fe doping, no apparent peaks related to iron oxide or any other impurities has been found suggesting that the Fe ions are successfully incorporated in the crystal structure of WO_3. This may be attributed to the lower concentration of Fe ions and small difference between the ionic radii of host W^{6+} (0.62 Å) and dopant Fe^{3+} (0.64 Å) ions. Hence, Fe^{3+} ions may easily be substituted for W^{6+} ions in the host matrix and forming Fe:WO_3 finite solid solution. Moreover, the W^{6+} is octahedral coordinated with O^{2-}. In iron oxides, the crystal field stabilization energy of Fe^{3+} is higher for octahedral orientation than for tetrahedral orientation [15]. Therefore, Fe^{3+} can fulfil the same coordination as that of W^{6+}.

Consequently, Fe:WO_3 film shows the same crystal structure as that of WO_3 film. Similar crystal structures were also observed by Han et al. [16]. The observed shift in peak positions of Fe:WO_3 films compared to WO_3 film, can be attributed to the small difference between the ionic radii of W^{6+} and Fe^{3+}. The ionic radius of Fe^{3+} is slightly greater than that of W^{6+} and this can cause slight distortion in the crystal lattice when WO_3 is doped with Fe, and consequently a shift in the diffraction peaks. Such distortions can also produce a number of defects in the film, making it a better candidate for gas sensor and biosensor. Grain size of 12–18 nm were determined for WO_3 and 2-10 at % Fe:WO_3 thin films.

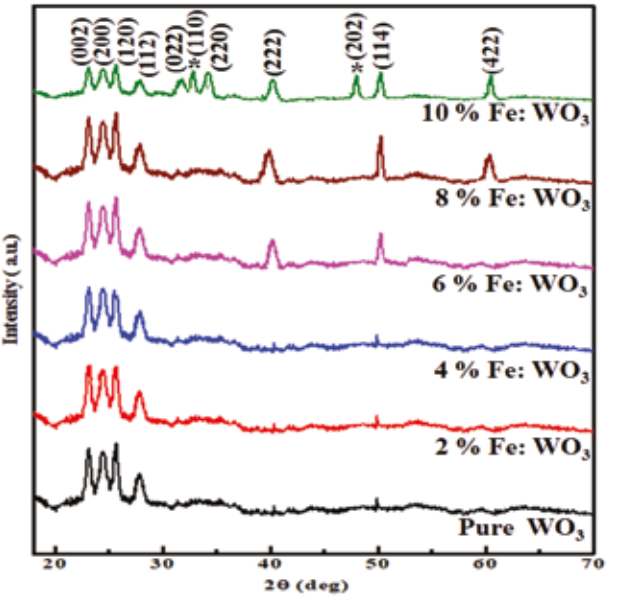

Figure 03: XRD patterns of Fe: WO_3 films at 0, 2, 6,8 and 10 at%, Fe concentrations.

3.4. Optical properties

The optical properties of the WO_3 and Fe :WO_3 films were measured in the wavelength range between 200 nm and 1100 nm. Figure 4 shows the optical transmittance spectra of WO_3 and Fe:WO_3 films. The absorption edge of undoped WO_3 and Fe:WO_3 films shifted to longer wavelengths indicating red shift. Maximum transmittance of undoped WO_3 lies between 25% and 35%. This low transmissions may be the effects of non-specular light scattering caused by the highly crystalline, granular and porous WO_3 thin films [17]. Fe-doped films showed lower transmittance compared to undoped films.

The transmittance of films depends on the structural, morphological and compositional characteristics of the films. From Figure 4 sharp absorption edge of the films can be observed below 400 nm. It is hypothesized that Fe can be introduced in small quantities as a substitutional impurity due to a small difference of ionic radius and this can cause distortion in the WO_3 crystal structure. Such lattice mismatch combined with the properties of the film and the type of strain induced into the film can produce either blue or red shift in the optical absorption.

Compressive strain can be expected in the films that would result a red shift in the optical absorption which would also influence the optical band gap energy of the films. The WO_3 and Fe:WO_3 films were found to be fairly transparent, having visible transmittance in excess of 82% for 4 at % Fe doping. it is well known that such transmission curves are associated with high concentrations of grain boundary defects that serve as electron-hole recombination sites. Consequently, the concentration of surface defects (relative to the total volume), which provide surface-active sites remains nearly constant while the volume, which contains recombination sites at the grain boundaries, continues to increase as the film thickness increases.

The optical band gaps (Eg) of the various films were evaluated from the transmittance spectra by plotting $(\alpha h\gamma)^2$ vs $h\gamma$ that is appropriate for an direct band gap material and then using linear extrapolation to the energy axis $(\alpha h\gamma)^2 = 0$. There is a slight decrease in the optical band gap when Fe was incorporate into the tungsten oxide film. The red shift observed in the optical absorption caused a negative shift (reduction) in the band gap of the WO3 film. The optical band gap of the Fe:WO_3 films obtained here are found to be within the ranges of optical band gap of the Fe:WO_3 films obtained by other earlier reported values [18].

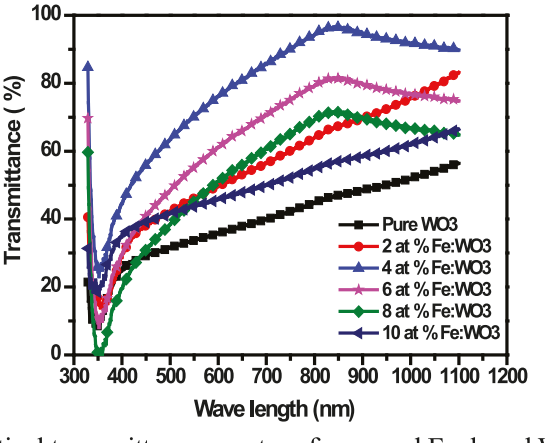

Figure 04: Optical transmittance spectra of pure and Fe doped WO_3 the films.

The band gap energy for pure WO_3 nanoparticles has been observed to be 2.72 eV which increased to 2.99 eV and 3.03 eV at 2 at % and 4 at% Fe doping and is decreased to 2.88eV, 2.79 eV and 2.74 eV with , 6 at%, 8 at% Fe and 10 at% Fe doping, respectively. This increase and decrease in the band energy of WO_3 nanoparticles can be understood the basis of hybridization between Fe 3d orbital and the O 2p orbital. As it is well known that in case of pristine WO_3, valance band is dominated by O 2p and conduction band is dominated by W 5d orbitals. But when Fe ions are introduced in the system, their 3d orbitals emerge around valance band and induce slight positive shift in it. Besides, Fe ions can also lead to downshift of conduction band. These corrections in the positions of valance and conduction bands lead to narrowing of the band gap which might help to harvest more visible light in it and generates more electron holes pairs.

3.5. Electrical properties

The room temperature electrical resistivity of undoped WO_3 thin films has been found to be 7.31 ×105 Ω-cm which decreases significantly on Fe doping. Decrease in resistivity with Fe dopant concentration may be attributed to incorporation of iron ions into WO_3 lattice, resulting in increase in oxygen vacancy i.e. carrier concentration. Also, based on the size effects of electrical conductivity, when the crystallite size is below ~15 nm, the grain boundary scattering decreases significantly and therefore increases the conductivity. This results satisfy the reported results by Lethy et al. and Whilst Patil et al. [19] temperature dependence of electrical resistivity of WO_3 thin films in the temperature range 300-423 K.

The decrease in resistivity with temperature indicates the semiconductor behavior of the films. In fact, resistivity is the result of trade-off between two competing processes occurring simultaneously, namely, thermal excitation of electrons and adsorption of atmospheric oxygen on the film surface. The electronic transport of WO_3, in general, is believed to be controlled by the hopping conduction process, and the electrons are the major carriers via the oxygen vacancies [20]. The effect of Fe concentrations on the properties of nanostructured WO_3 thin films are summarized in Table 1.

Table 01: Effect of Fe concentration on the properties of WO_3 thin films.

Thin films	Thickness ± 10 nm	Crystallite size, D (nm)	Optical band gap Eg (eV)	Electrical resistivity ρ Ω-cm)
Pure WO_3	288	13	2.72	7.31×10^5
2 at % Fe:WO_3	276	11	2.99	7.89×10^5
4 at % Fe:WO_3	269	8	3.03	6.56×10^5
6 at % Fe:WO_3	261	10	2.88	6.17×10^5
8 at % Fe:WO_3	256	12	2.79	5.93×10^5
10 at % Fe:WO_3	251	15	2.74	5.78×10^5

4. CONCLUSIONS

Transition metal oxide viz. WO_3 thin films were synthesized by spray pyrolysis technique. Effect of Fe doping concentration on morphological, elemental, structural, optical and electrical properties of WO_3 were studied. The surface homogeneity of the deposited films increases with Fe content due to the effect of friction among the charge carriers. XRD patterns indicated that the Fe ions replaced W ions without changing the structure. Small crystallite size, regularity of surface morphology, high transmittance, and tunable band gap, high conductivity, of Fe doped WO_3 thin films suggest the suitability of the material in optoelectronic devices and bio sensing applications.

REFERENCES

[1] Tian K, Prestgard M and Tiwari A 2014 A Review of Recent Advances in Nonenzymatic Glucose Sensors Materials Science and Engineering C 41 pp 100-118 .

[2] Marie M, Mandal S and Manasreh O 2015. An Electrochemical Glucose Sensor Based on Zinc Oxide Nanorods Sensors 15 pp 18714-18723 .

[3] C.Santato, M.Odziemkopwski, M.Ulmann and J.Augustynski "Crystallographically Oriented Mesoporous WO3 Films: Synthesis, Characterization, and Applications", J. Am. Chem. Soc. 123, pp. 10639-10649, 2001.

[4] D.Z. Guo, K. Yu-Zhang, A. Glote, G.M. Zhang and Z.Q Xue "Synthesis and Characterization of Tungsten Oxide Nanorods", J. Mater. Res., (19) pp. 3665-3670, 2004.

[5] C. G. Granqvist, Sol. Energy Mater. Sol. Cells 60, 201 _2000_.

[6] R. G. Bamwenda, K. Sayama, and H. Arakawa, J. Photochem. Photobiol., A 122, 175 1999.

[7] J.M. O-Rueda de Leon, D.R. Acosta, U. Pal, and L. Castaneda, Improving Electrochromic Behavior of Spray Pyrolised WO3 Thin Solid Films by Mo Doping, Electrochim. Acta, 2011, 56, p 2599–2605 .

[8] Z Hu, S Haneklaus, G Sparovek and E Schnug Commun. Soil. Sci. Plant. Anal. 37 1381 (2006) .

[9] Y. Liu, Y. Li, W. Li, S. Han, C. Liu, Photoelectrochemical properties andphotocatalytic activity of nitrogen-doped nanoporous WO3 photoelectrodesunder visible light, Appl. Surf. Sci. 258 (12) (2012) 5038–5045.

[10] P.R. Patil, P.S. Patil, Preparation of mixed oxide MoO3 –WO3 thin films by spray pyrolysis technique and their characterization, Thin Solid Films 382 (2001). 13-22.

[11] Woodward PM, Sleight AW, Vogt T. Structure refinement of triclinic tungsten trioxide. J Phys Chem Solids; 1995, 56 (10):1305-315.

[12] S.C. Moulzolf, L.J. LeGore, R.J. Lad, Heteroepitaxial growth of tungsten oxide films on sapphire for chemical gas sensors, Thin Solid Films 400 (2001) 56–63.

[13] R.M. Cornell, U. Schwertmann, The Iron Oxides: Structure, Properties, Reactions, Occurrences and Uses, 2nd ed., Wiley-VCH, Verlag GmbH & Co, 2003.

[14] N. Han, L. Chai, Q. Wang, Y. Tian, P. Deng, Y. Chen, Evaluating the doping effect ofFe, Ti and Sn on gas sensing property of ZnO, Sensors and Actuators B: Chemical 147 (2010) 525–530.

[15] Wang, F.,Di Valentin, C.; Pacchioni, G., Doping of WO3 for Photocatalytic Water Splitting:Hints from Density Functional Theory, J. Phys. Chem. C 116 (2012) 8901-8909.

[16] Zook JD. Effects of grain boundaries in polycrystalline solar cells. Appl Phys Lett 1980;37 (2) : 223-26.

[17] J. Tauc, Amorphous and Liquid Semiconductors, Plenum Press, London, 1974.

[18] A.Z. Moshfegh, R. Azimirad, O. Akhavan, Optical properties and surfacemorphology of evaporated WO3-Fe2O3 thin films, Thin Solid Films 484 (2005) 124–131.

[19] D.V. Fedorov, P. Zahn, and I. Mertig, Size Effects and Conductivity of Ultrathin Cu Films, Thin Solid Films, 2005, 473, p 346-350.

[20] K.J. Lethy, D. Beena, V.P.M. Pillai, and V. Ganesan, Bandgap Renormalization in Titania Modified Nanostructured Tungsten Oxide Thin Films Prepared by Pulsed Laser Deposition.

Particulate matter (PM), especially PM10 and PM2.5, can harm children, people with chronic health problems, and asthma sufferers [1, 2]. Carbon monoxide (CO) exposure can cause a variety of health problems, including mental impairment, lung edema, and heart problems [3]. Ammonia (NH_3) exposure can irritate the throat and eyes, cause coughing and phlegm production, and contribute to asthma and chronic lung problems [4]. Benzene (C_6H_6) exposure, mainly from smoking, can affect the immune, reproductive, neurological, endocrine, cardiovascular, and respiratory systems [5].

2. IoT MOTIVATION AND SYSTEMS REVIEW

2.1. Motivation

Almost one in nine fatalities worldwide is caused by air pollution, making it one of the most significant environmental hazards to health [6]. The atmosphere's largest cause for concern, both for the ecosystem and public health in terms of lung and heart problems, is air pollution. Bangladesh, as the world's most populated and developing third-world country, faces increasing challenges in combating air pollution [7]. Awareness of the adverse effects of chemical pollutants has grown substantially in recent years, prompting increased efforts to understand and address environmental pollution. Accurate information and comprehensive toxicological research are essential for guiding further investigation. This study contributes to this growing body of knowledge by proposing practical methods to measure and mitigate air pollution's harmful impacts, aiming to promote a healthier and more sustainable future. In response to the global concerns surrounding air quality and public health, an IoT-based air pollution monitoring system is proposed. This system tracks pollutants such as Carbon monoxide (CO), Carbon dioxide (CO_2), Ammonia (NH_3), Sulfide, PM2.5, and PM10 in real-time, providing valuable data for decision-making [8]. Operating in online, offline, and real-time modes, the system ensures continuous monitoring and data recording, enhancing understanding of air quality dynamics. Additionally, the integration of solar power and GPS technology enables operation in remote areas and precise location tracking during data collection.

In this section, we will examine several additional IoT systems that have inspired the implementation of the project. The table provides a comparison between our IoT system and other notable IoT systems. The primary contributions of our project are outlined below:

UITS Journal of Sciences & Engineering ❖ Volume-10, Issue-1
ISSN: 2521-8107; March 2024

Revolutionizing Air Quality Monitoring: A Comprehensive IoT-Based Approach

Md. Ashraful Islam[1], *Mir Md. Mosarof Hossan Showrav[2], Sumaiya Nurim[3]

ABSTRACT: In response to escalating global concerns surrounding air quality, this paper introduces an innovative IoT-based system for comprehensive air quality monitoring. By integrating advanced sensor technology with real-time data transmission, this system offers unprecedented accuracy and accessibility in air quality data, thereby facilitating informed decision-making for researchers, policymakers, and public health officials. The system's design and implementation details, along with its effectiveness under various environmental conditions, are discussed in depth.

Keywords: Air pollution, IoT, Particulate matter, Real-time monitoring, Solar power.

1. INTRODUCTION

The deterioration of air quality has become a critical issue worldwide, prompting the need for advanced monitoring systems. Traditional methods often lack the granularity and real-time data necessary for effective intervention. This study aims to address these limitations by leveraging Internet of Things (IoT) technology to provide continuous and precise air quality measurements.

Objectives and Rationale: This paper specifically targets researchers, policymakers, and public health officials who require accurate, real-time data to make informed decisions regarding air quality management. By addressing the needs of these groups, the system aims to enhance public health outcomes and environmental policy.

The system focuses on tracking harmful gases like carbon monoxide (CO), carbon dioxide (CO_2), ammonia (NH_3), sulfide, benzene (C_6H_6), and particulate matter (PM2.5 and PM10) while also monitoring temperature and humidity. To address these serious health risks, this paper proposes a novel IoT system for real-time air quality monitoring and data collection.

1 Professor, Department of CSE, UITS
Email: ashraful47@uits.edu.bd, ashraful47@yahoo.com
2 Research Fellow, Department of CSE, UITS
* Corresponding Author: Email: showravofficial@gmail.com
3 Research Fellow, Department of CSE, UITS
Email: nurimsumaiya207@gmail.com

1. Design and implement an IoT-based air pollution monitoring system.
2. Development of a monitoring system using cloud storage and ESP32 Wi-Fi for secure data handling.
3. Utilization of IoT technology for real-time tracking of pollutants.
4. Integration of solar power and GPS technology for enhanced functionality, enabling remote operation and precise location tracking during data collection.
5. Implement a handy, cost-efficient and low-power consumed IoT system.

2.2. Related works

In [8], Mohana and Malleswari underscore the importance of IoT devices for real-time air quality monitoring, integrating sensors with platforms like Arduino and Raspberry Pi to enable comprehensive data collection and pollution mitigation efforts.

In [9], Fann, Neal, et al. focus on assessing the health impacts of ground-level ozone (O_3) and fine particulate matter (PM2.5) concentrations in the United States for the year 2005. The study uses the Community Multiscale Air Quality (CMAQ) model and monitored data to create detailed spatial maps of these air pollutants.

Aashiq explores the weather-air quality nexus, introducing a portable IoT device measuring multiple parameters for real-time monitoring via a mobile app and ThingSpeak cloud platform, promising widespread deployment potential. [10].

In [11], Kortoçi et al. advocates a citizen-based monitoring system employing low-cost sensors for PMs, CO_2, and NOx to empower public awareness and policy-making for cleaner air. Their approach provides personalized pollution data, demonstrating sensor accuracy comparable to that of high-end stations.

Dhingra et al. propose a three-phase IoT air pollution monitoring system with gas sensors and Wi-Fi for data transmission. Their system includes an Android app, IoT-Mobair, providing real-time air quality data, route predictions, and health risk assessments, akin to Google Traffic[12].

In [13], Binsy and Sampath introduce an IoT-based smart air pollution monitoring device with user-configurable settings, sensors, a Raspberry Pi 3, and GPS for data collection, accessible via a Bluetooth-enabled Android app and the ThingSpeak IoT platform.

In [14], Kim, Ki-Hyun, Ehsanul Kabir, and Shamin Kabir highlight the health risks of particulate matter (PM) from natural and human activities, emphasizing the need for detailed knowledge to inform policymakers.

Parmar, Gagan, Sagar Lakhani, and Manju K. Chattopadhyay designed an environmental air pollution monitoring system using affordable nodes with Wi-Fi and semiconductor gas sensors to track CO, CO_2, SO_2, and NO_2 [15].

In [16], Tapashetti, Vegiraju, and Ogunfunmi propose a low-cost indoor air monitoring device focusing on CO and HCHO, with scalability for emissions monitoring, facilitating real-time cloud communication and aiding comprehension of air quality dynamics.

Al Nahian et al. link high air pollution in Dhaka to increased rates of preterm births and low birth weight, highlighting alarming pollution levels contributing to elevated risks, notably affecting female fetuses for LBW and males during the second trimester for PTB [17].

In [18], Das et al. introduce an IoT-based Air Pollution Monitoring Device (APMD) with PM 2.5, PM 10, CO, SO_2, NO_2, ozone sensors, and environmental parameters. It utilizes solar energy, and a rechargeable battery transmits data via Wi-Fi/NB-IoT, incorporates GPS for location, and shows accuracy in a 7-day field test, vital for urban air quality monitoring.

In [19]. Shaban, Khaled Bashir, Abdullah Kadri, and Eman Rezk introduce an urban air pollution monitoring and forecasting system leveraging low-cost sensors and the M5P algorithm for accurate predictions, crucial for alert systems in highly polluted areas.

In [20], Ayelee, Temesegan Walelign, and Rutvik Mehta. introduce an Internet of Things (IoT) based system for monitoring and predicting air pollution. The proposed system aims to monitor air pollutants in specific areas, analyze air quality, and forecast air quality conditions.

Hussain, Ayaz, et al. introduce an IoT-based smart bin system that not only manages waste but also forecasts air pollutant levels in the vicinity of the bin. And they predicted the status of the bin and the concentration of carbon monoxide (CO) in the air [21].

In [22], Esfahani et al. unveils a low-cost IoT indoor air quality monitoring system with sensors for VOCs, CO_2, PM2.5, PM10, temperature, humidity, and illuminance, interfacing with a Blynk app for EPA-based air quality index computation, enhancing indoor air quality.

3.2. Hardware Requirements

Table 02: Components used in the device.

Categories	Components
Microcontroller Boards	• Arduino Mega 2560 CH340. • ESP32 ESP-32S 30PNodeMCU Development Board Wireless Wi-Fi.
Gas Sensors	• MQ-135 Gas Sensor. • Dust Sensor DSM501A Air Quality Monitoring. • MQ-7 Carbon Monoxide Gas Sensor.
Environmental Sensors	• DHT11 Digital Temperature humidity Sensor Module.
GPS and Location	• NEO-M8N GPS Module with Ceramic Active Antenna.
Power and Charging	• 18650 Li-ion Rechargeable Battery (Blue). • 18650 Battery Holder 3S with wire. • DC Barrel Power Jack Plug Connector 2.1mm x 5.5mm x 9mm. • TP4056 Lithium Battery Charger Module with Protection Dual Functions.
Display and Output	• 16x2 Serial LCD Module Display for Arduino Assembled. • LED 5mm.
Connectivity and Wiring	• Jumper Wire Single 20cm - Jumper Wire Type: (Male to Female, Male to Male, Female to Female). • Mini Breadboard. • MicroSD Card Module.
Energy Harvesting	• Round Solar Panel.
Resistor	• 220 Ω (ohm) resistor

3.4. Index of Air Quality Data

Table 03: PM2.5, PM10 and CO Index [23].

AQI Category	PM2.5	PM10	CO
Good	0 – 30	0 – 50	0 – 1.0
Satisfactory	31 – 60	51 – 100	1.1 – 2.0
Moderately polluted	61 – 90	101 – 250	2.1 – 10
Poor	91 – 120	251 – 350	10 – 17
Very poor	121 – 250	351 – 430	17 – 34
Severe	250+	430+	34+

Table 01: Comparison of some promising existing systems with our system.

Existing systems	Comparison with our system
Parmar, Gagan, et al. (2017) [15]	[15] Parmar, Gagan, et al. designed an environmental air pollution monitoring system using affordable, low-cost nodes with Wi-Fi and semiconductor gas sensors. This system proposes a low-cost system to monitor air quality. On the other hand, we propose a low-cost, handly device by implementing Arduino Mega instead of Raspberry Pi, which is more cost-effective.
Kortoçi et al. (2022) [11]	In [11], Kortoçi et al. propose a citizen-based monitoring system employing low-cost sensors for PMs, CO2, and NOx to empower public awareness and policy-making for cleaner air. However, this system has no cloud-based storage system to store the sensor's data. Our proposed system has a cloud-based storage system to monitor and store real-time data.
Das et al. (2022) [18]	[18] Das, Ghosh, Chatterjee, and De present an IoT-based Air Pollution Monitoring Device (APMD) equipped with sensors for PM 2.5, PM 10, CO, SO2, NO2, ozone, and environmental parameters. In comparison, our proposed system extends beyond by incorporating additional parameters such as ammonia, benzene, and sulfide. Additionally, our system features a solar-powered system with a rechargeable battery and includes PM2.5 and PM10 sensors.
Kim, Ki-Hy un et al. (2015) [4]	In [4], Kim, Ki-Hyun, Ehsanul Kabir, and Shamin Kabir underscore the health hazards associated with particulate matter (PM). While their system focuses solely on monitoring PM in the environment, our proposed system offers broader functionality by also enabling the monitoring of hazardous gases in addition to particulate matter.

3. REQUIREMENTS AND SYSTEM OVERVIEW

3.1. Software Requirements

- Microsoft Windows 11 or later.
- Arduino IDE.

Table 04: MQ135 gas sensor Index [24].

AQ	AQI (ppm)
Good	0-50
Moderate	51-100
Unhealthy to sensitive group	100-150
Unhealthy	151-200
Very unhealthy	201-300
Hazardous	301-500

Table 05: Humidity & Temperature Index [25].

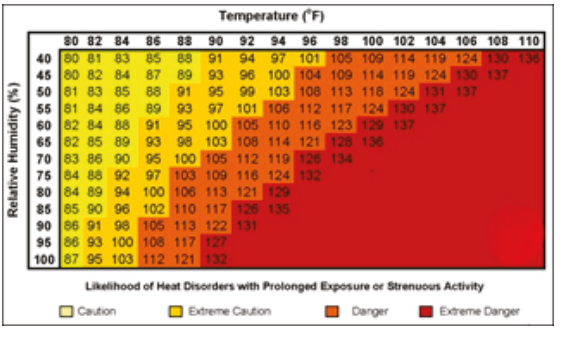

3.5. Design Diagrams

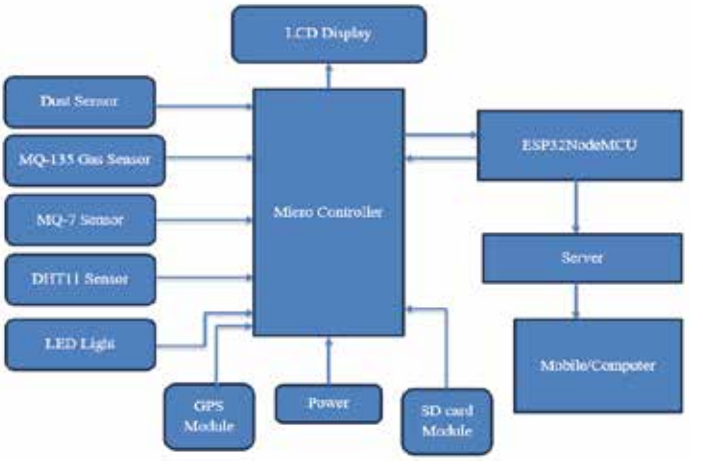

Figure 01: System Block diagram.

3.6. Dataflow Diagram

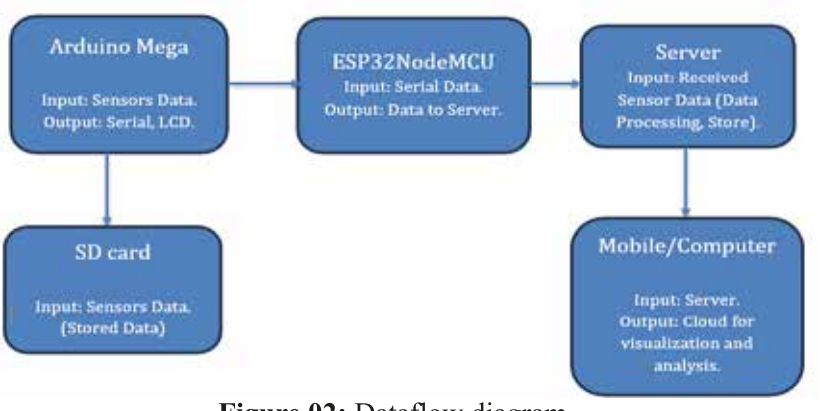

Figure 02: Dataflow diagram.

3.7. Flowchart of the control algorithm

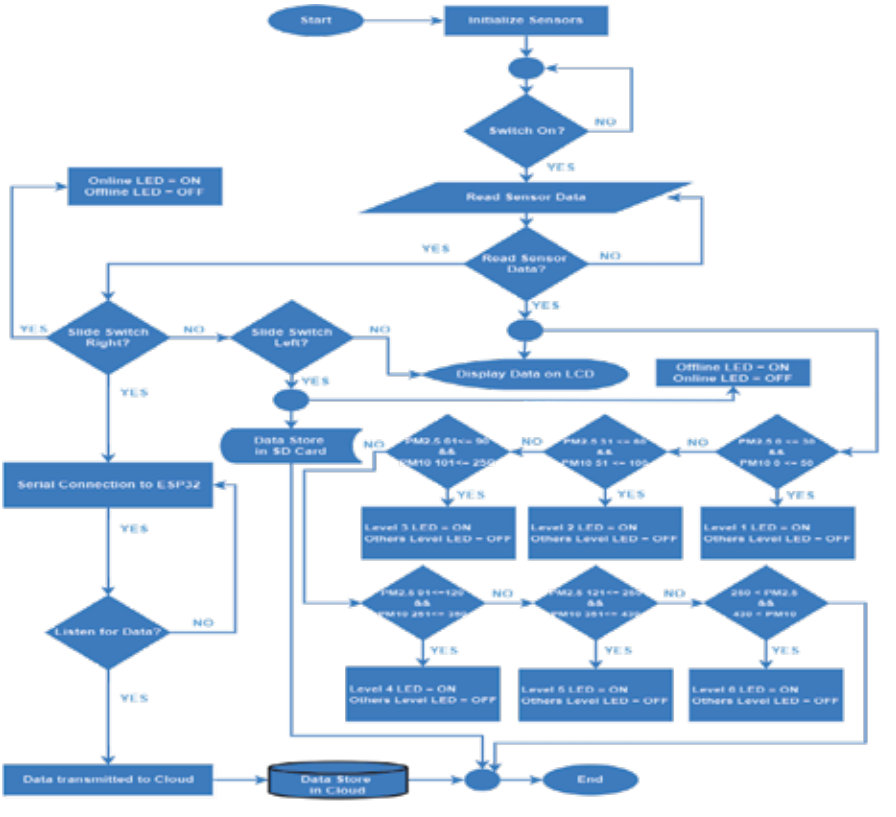

Figure 03: Flowchart for system operation.

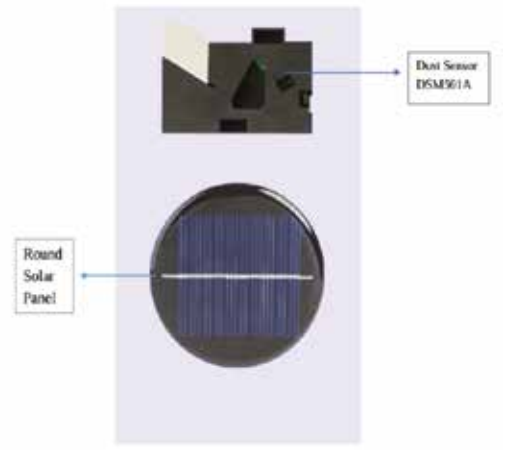

Figure 06: System model back side view.

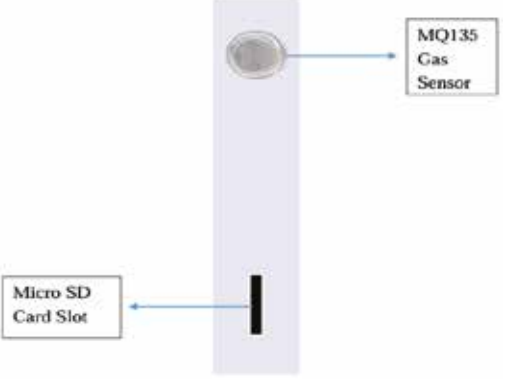

Figure 07: System model left side view.

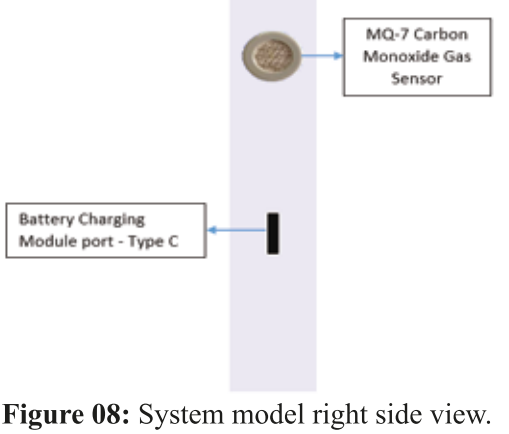

Figure 08: System model right side view.

4. SYSTEM DESIGN AND IMPLEMENTATION

4.1. Wiring instruction

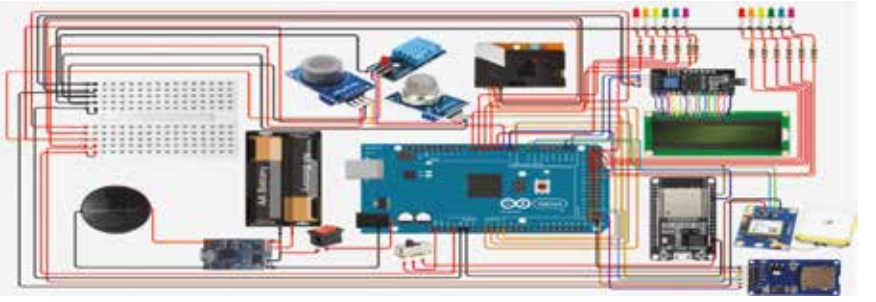

Figure 04: Circuit Diagram.

The proposed IoT-based air pollution monitoring system comprises various sensors, including DSM501A, MQ135, MQ7, DHT11, MicroSD card module and GPS which are connected to the Arduino Mega. Also, some LEDs are added to sense the dust level in the air. A solar panel and rechargeable battery ensure continuous operation, while an ESP32NodeMCU facilitates online data transmission. The detailed wiring instructions and circuit diagram, presented in Fig. 4, guide the implementation process. Additionally, the system's power supply and its comparison with existing systems highlight its cost-effectiveness and innovative features.

4.2. System Model

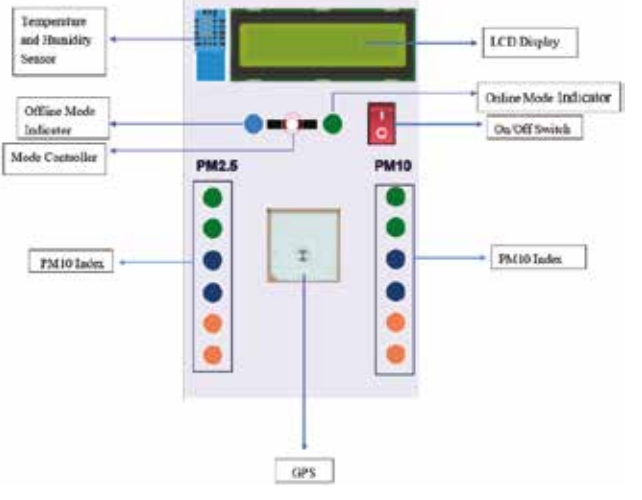

Figure 05: System model front side view.

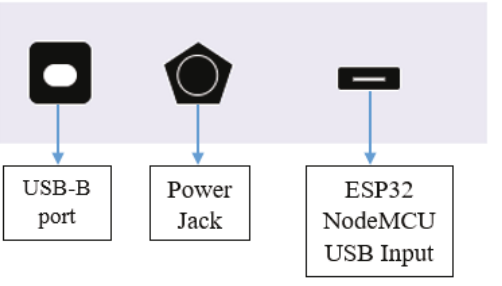

Figure 09: System model down side view.

4.3. Mathematical model

The MQ-135 gas sensor resistance (Rs) is given by the equation:

$$Rs = \left(\frac{V_C}{V_{RL}} - 1\right) \times R_{RL} \qquad (1)$$

where Rs is the sensor resistance, V_C is the supply voltage to the sensor, V_{RL} is the voltage across the load resistance, and R_{RL} is the load resistance.

Specifications/Characteristics	Image
• Operating Voltage: 2.5V to 5.0V • Power consumption: 150mA • Detect/Measure: NH_3, Nox, CO_2, Alcohol, Benzene, Smoke. • Typical operating Voltage: 5V • Analog & Digital Output: 0V to 5V (TTL Logic) 5V Vcc.	

Figure 10: Image and specifications of the MQ-135 sensor.

The DHT11 sensor provides temperature (T) and humidity (H) readings through a 40-bit data stream.

$$H = \text{DecimalHumidity}\left(\frac{IntegerHumidity}{10}\right) \qquad (4)$$

$$T = \text{DecimalTemperature}\left(\frac{IntegerTemperature}{10}\right) \qquad (5)$$

where DecimalHumidity, IntegerHumidity, DecimalTemperature, and IntegerTemperature are obtained from the sensor's data stream. This allows for accurate conversion of the digital output into meaningful temperature and humidity values for environmental monitoring applications.

Specifications/Characteristics	Image
• Operating Voltage: 3.5V to 5.5V • Operating current: 0.3mA (measuring) 60uA (standby) • Output: Serial data • Temperature Range: 0°C to 50°C • Humidity Range: 20% to 90% • Resolution: Temperature and Humidity both are 16-bit • Accuracy: ±1°C and ±1%.	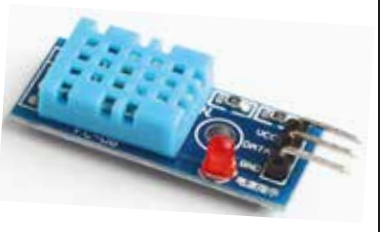

Figure 11: Image and specifications of the DHT11 sensor.

Similar to MQ-135, the MQ-7 gas sensor resistance (Rs) is given by the equation:

$$Rs = \left(\frac{V_C}{V_{RL}} - 1\right) \times R_{RL} \qquad (2)$$

where Rs is the sensor resistance, V_C is the supply voltage to the sensor, V_{RL} is the voltage across the load resistance, and R_{RL} is the load resistance.

Specifications/Characteristics	Image
• Operating voltage (v) DC 5. • Range 10 ~ 1000 ppm. • Characteristic gas 100 ppm CO. • Sensitivity ≥ 3%. • Return time ≤ 30 sec. • Heating resistance ± 31 Ω. • Heating current ≤ 180 mA. • Heating voltage 5.0V ±2V / 1.5 ± 1V • Heating power approx. 350m W • Ambient temperature (°C) -20~+ 50. • Humidity ≤ 95% RH • Oxygen content 21%. • Length (mm) 35. • Width (mm) 20. • Height (mm) 11. • Weight (gm) 20. • Shipment Weight 0.01 kg. • Shipment Dimensions 4 x 4 x 4 cm.	

Figure 12: Image and specifications of the MQ-7 sensor.

The particle concentration (C) from DSM501A is modeled by:

$$C = \frac{K.V}{V_{ref}} \qquad (3)$$

where C is the particle concentration, K is the sensitivity factor, V is the output voltage of the sensor, and V_{ref} is the reference voltage.

Specifications/Characteristics	Image
• Operating Voltage Range: DC 5V ± 0.5V. • Output Mode: PWM (Pulse Width Modulation). • Output Voltage: Low Level (with particles): 0.7V (max. 1.0V). High Level (clean air): 4.5V (min. 4.0V). • Smallest Particle Measure :1um. • Sensitivity:15,000 / 283 ml. • Operating Current (Max): 90mA. • Humidity Range: Storage Environment: 0-99% RH. Working Environment: 0-95% RH. • Temperature Range: Storage Environment: -20°C to 80°C. Working Environment: -10°C to 60°C.	

Figure 13: Image and specifications of the DSM501A sensor.

5. LIMITATIONS OF THIS PROJECT

The system has been intrigued by the GPS module, which sometimes takes time to connect in challenging environments. The MQ135 gas sensor has a limitation in accurately distinguishing between specific gases, as it is sensitive to a range of pollutants and may need to provide precise identification of individual gases in complex environments. The project encounters occasional data transfer challenges stemming from internet disruptions affecting cloud data transmission. It relies on Google Cloud to store real-time data from air quality sensors, which poses concerns regarding data ownership and reliability.

6. FURTHER DEVELOPMENTS

In future developments, the project aims to develop a software solution based on machine learning techniques that will offer user-friendly access to comprehensive weather data for various locations. Additionally, the system will provide insights into potential environmental health risks, elucidating the correlation between environmental factors and prevalent diseases.

Through cloud-based storage of air quality data, the system ensures its availability for future research endeavors. Furthermore, the envisioned software will provide distinct visualization of gas detection results, particularly focusing on individual sensors such as the MQ135 gas sensor. Alongside this, the project aims to set up a network to help people learn more about pollution. It will encourage more people to care about the environment and get involved in efforts to protect it.

7. CONCLUSIONS

The proposed IoT-based air pollution monitoring system offers a holistic approach to addressing global concerns. By combining technological advancements like solar power and GPS with real-time tracking capabilities, the system aims to revolutionize air quality monitoring. The emphasis on cloud-based data storage ensures informed decision-making and sustainable air quality management, promoting community well-being and a healthier future.

In conclusion, this article provides a comprehensive overview of the proposed IoT-based air pollution monitoring system, emphasizing its innovative features, capabilities, and future development prospects. The integration of advanced technology, cost-effectiveness, and user-friendly design positions this system as a potential game-changer in the field of environmental monitoring.

REFERENCE

[1] Fuller, Richard, et al. "Pollution and health: a progress update." The Lancet Planetary Health 6.6 (2022): e535-e547.

[2] Mukherjee, Arideep, and Madhoolika Agrawal. "World air particulate matter: sources, distribution and health effects." Environmental chemistry letters 15 (2017): 283-309.

[3] Abelsohn, Alan et al. “Identifying and managing adverse environmental health effects: 6. Carbon monoxide poisoning.” CMAJ : Canadian Medical Association journal = journal de l'Association medicale canadienne vol. 166,13 (2002): 1685-90.

[4] Wyer, Katie E., et al. "Ammonia emissions from agriculture and their contribution to fine particulate matter: A review of implications for human health." Journal of Environmental Management 323 (2022): 116285.

[5] Bahadar, Haji, Sara Mostafalou, and Mohammad Abdollahi. "Current understandings and perspectives on non-cancer health effects of benzene: a global concern." Toxicology and applied pharmacology 276.2 (2014): 83-94.

[6] World Health Organization. "Ambient air pollution: A global assessment of exposure and burden of disease." (2016).

[7] Sathi, Sayma, et al. "EFFECTS OF METEOROLOGICAL PARAMETERS ON PRIMARY AIR POLLUTANTS: CASE STUDY AT DHAKA (CAMS-3, DARUS-SALAM)."

[8] Malleswari, S. M. S. D., and T. Krishna Mohana. "Air pollution monitoring system using IoT devices." Materials Today: Proceedings 51 (2022): 1147-1150.

[9] Fann, Neal, et al. "Estimating the national public health burden associated with exposure to ambient PM2. 5 and ozone." Risk Analysis: An International Journal 32.1 (2012): 81-95.

[10] Aashiq, M. N. M., et al. "An IoT-based handheld environmental and air quality monitoring station." Acta IMEKO 12.3 (2023): 1-9.

[11] Kortoçi, Pranvera, et al. "Air pollution exposure monitoring using portable low-cost air quality sensors." Smart health 23 (2022): 100241.

[12] Dhingra, Swati, et al. "Internet of Things mobile–air pollution monitoring system (IoT-Mobair)." IEEE Internet of Things Journal 6.3 (2019): 5577-5584.

[13] Binsy, M. S., and Nalini Sampath. "User configurable and portable air pollution monitoring system for smart cities using IoT." International Conference on Computer Networks and Communication Technologies: ICCNCT 2018. Springer Singapore, 2019.

[14] Kim, Ki-Hyun, Ehsanul Kabir, and Shamin Kabir. "A review on the human health impact of airborne particulate matter." Environment international 74 (2015): 136-143.

[15] Parmar, Gagan, Sagar Lakhani, and Manju K. Chattopadhyay. "An IoT based low cost air pollution monitoring system." 2017 International Conference on Recent Innovations in Signal processing and Embedded Systems (RISE). IEEE, 2017.

[16] Tapashetti, Akshata, Divya Vegiraju, and Tokunbo Ogunfunmi. "IoT-enabled air quality monitoring device: A low cost smart health solution." 2016 IEEE Global Humanitarian Technology Conference (GHTC). IEEE, 2016.

[17] Al Nahian, Mahin, et al. "Air pollution and pregnancy outcomes in Dhaka, Bangladesh." The Journal of Climate Change and Health 9 (2023): 100187.

[18] Das, Payali, et al. "A low cost outdoor air pollution monitoring device with power controlled built-in PM sensor." IEEE Sensors Journal 22.13 (2022): 13682-13695.

[19] Shaban, Khaled Bashir, Abdullah Kadri, and Eman Rezk. "Urban air pollution monitoring system with forecasting models." IEEE Sensors Journal 16.8 (2016): 2598-2606.

[20] Ayele, Temesegan Walelign, and Rutvik Mehta. "Air pollution monitoring and prediction using IoT." 2018 second international conference on inventive communication and computational technologies (ICICCT). IEEE, 2018.

[21] Hussain, Ayaz, et al. "Waste management and prediction of air pollutants using IoT and machine learning approach." Energies 13.15 (2020): 3930.

[22] Esfahani, Siavash, et al. "Smart city battery operated IoT based indoor air quality monitoring system." 2020 IEEE SENSORS. IEEE, 2020.

[23] Chundawat, Charushree . "AQI Index - EXPLAINED: What Is Air Quality Index and How It Is Calculated? What Are Necessary Precautions against Pollution." Zee Business, 4 Nov. 2022, www.zeebiz.com/india/news-aqi-index-explained-what-is-air-quality-index-and-how-it-is-calculated-what-are-necessary-precautions-against-pollution-204128. Accessed 19 Dec. 2023.

[24] Rani, SHOLA USHA, et al. "Real-Time Air Quality Monitoring System Using MQ-135 and Thingsboard." Journal of critical reviews 7.18 (2020): 4107-4115.

[25] Weather.gov. "Heat Index." National Weather Service, n.d. Web. 5 Jan. 2024. https://www.weather.gov/ama/heatindex.